Polymer Bulletin 28, 235–242 (1992)

Polymer Bulletin

Analysis of a PS/PMMA blend by image processing techniques

A. Godart, R. Schirrer, and C. Wippler*

Institut Charles Sadron (EAHP-CRM), 4 rue Boussingault, F-67000 Strasbourg, France

Abstract

Concepts of image analysis by mathematical morphology were applied to the characterization of the morphology of an incompatible polymer blend (PS/PMMA) processed on an extruder. The morphologies originated from the breakup of particles according to a Rayleigh mechanism. We tried to estimate the initial length and radius of fibers using a specific particle *labelling* to check if the Tomotika's relation between the fiber radius and the characteristic length associated with breakup was, in our case, verified. The *covariance function*'s method was also applied. More generally, the contribution of mathematical morphology to polymer morphology characterization was outlined.

1. Introduction

Most polymeric blends are multiphase systems and, as such, their properties largely depend on their morphologies. In establishing the relationship between physical properties and morphologies, one has to face the problem of finding suitable characteristics of the morphologies. This problem has not been adequately solved until now. Over past years the image processing techniques have progressed considerably, so it has become quite normal to try to apply them for the characterization of blend morphologies. Investigations along this line have already been published (1,2,3). Generally, these publications describe progressive changes of morphology. For example, two distinct phases can be seen to appear during spinodal decomposition. These alterations of morphology can be followed either by observing the changes in the shape of the power spectrum of the two dimensional fast Fourier transform (1,2), or by computing the amplitude of the *gradient image* (3). A recent use of mathematical morphology in three dimensions for an analysis of a polyurethane foam is described in (4).

In this paper we wanted to report some of the results we have obtained with polystyrene/polymethylmethacrylate blends using concepts of image analysis by mathematical morphology. The rheological behavior of such blends of various compositions, with and without a compatibilizing agent, has already been published (5). For this study we used the *commercial software Visilog*. Words in italic are shortly explained in appendix A. For more precise informations see the reference books (6,7,8)

2. Experimental part

The two homopolymers used are commercial products (5,9):

- Polystyrene (PS) was PNBOO (from ORKEM), mean molecular weight $M_n = 125\ 000$ g.mol^{-1} and index of polydispersity I=2.44
- Polymethylmethacrylate (PMMA) was DIAKON MG 102 (from ICI), mean molecular weight $M_n = 44\ 000$ g.mol^{-1} and index of polydispersity I= 2.32

*To whom offprint requests should be sent

We will restrict ourselves to only one composition of a PS/PMMA blend without compatibilizer: a blend of weight composition 25% PS and 75% PMMA.

The blend was processed on a Clextral twin-screw extruder, model BC21. The screws were corotative and equipped with two mixing zones. The die had a length of 25 mm and a diameter of 3 mm. The temperatures along the barrel were set to 200°C and to 210°C for the die. At the exit of the die, the extrudate was immediately quenched in water.

Although we have taken many other micrographs, we have only commented on those reproduced here, for a sake of clarity.

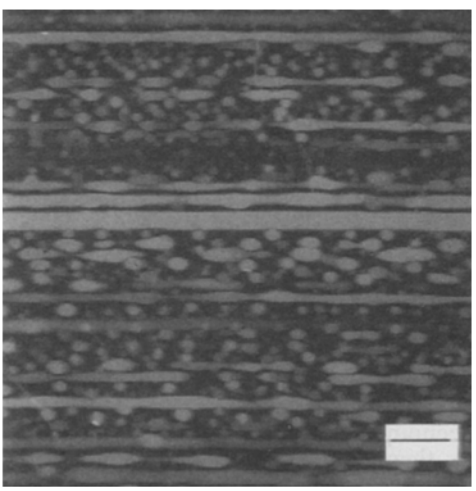

Figure 1: Transmission electron microscope observation parallel to the extrusion direction (scale is corresponding to 1 μm)

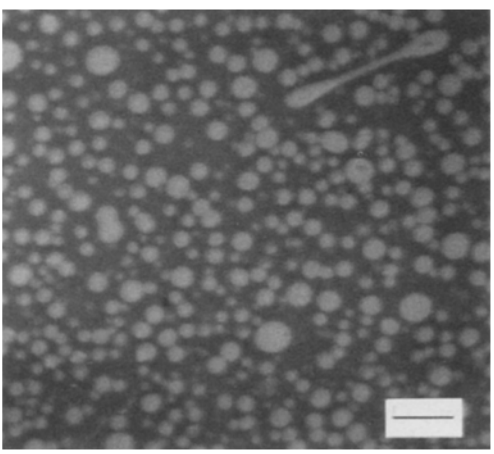

Figure 2: Transmission electron microscope observation perpendicular to the extrusion direction (scale is corresponding to 1 μm)

The transmission electron micrographs (figure 1 and 2) were taken, parallel and perpendicular to the extrusion direction (the samples were ultramicrotomed near the central axis of the extrudate). The micrographs clearly show, in white, the PS phase dispersed as fibers or elongated particles embedded in the PMMA matrix. The fiber's and particle's axes were parallel to each other.

A visual observation of figure 1, led to the conclusion that elongated particles can be sorted into families of particles aligned in a parallel direction to the fiber axes. Each family was judged the result of the fragmentation of a single fiber. That was not unexpected as it is well known from Tomotika's work (10,11), who carried on Rayleigh's initial work (12,13), that viscous fibers embedded in a viscous medium are usually unstable under static conditions and are fragmented in equidistant particles. With time, these particles adopt a spherical shape.

We assumed that the distance between two centers of two neighboring particles could be taken equal to the distance, λ, for which the probability of breaking up is maximal. The relation between λ and the radius of the mother fiber, R_o, has been calculated by Tomotika as:

$$\lambda = A R_o \qquad (1)$$

A is a coefficient that is dependent on p, which is the ratio of the viscosity of the dispersed phase to the viscosity of the matrix. In our experience (p=0.4), the value of A could be estimated as 10.4. Consequently we had:

$$\lambda = 10.4\, R_o \qquad (2)$$

3. Analysis of morphology by image analysis

3.1. Analysis using a specific *labelling* of particles

3.1.1. a) *Binarization* of image of figure 1

The first operation consisted in transforming the initial image in figure 1 into the *binary image* which is shown in figure 3. *A top-hat transformation* permitted to provide a greater contrast. The image was then *thresholded* in two levels: level 1 (set in black on figure 3) corresponded to the particles of dispersed PS, level 0 (set in white on figure 3) corresponded to the matrix of PMMA.

Particles showed shape irregularities, more noticeably on the *binary image* than on the original image. In addition, some alignments of particles partially overlapped. Although there was evidence for an alignment of particles, it was not always easy to identify clearly, to the naked eye, a particle as born from a given fiber.

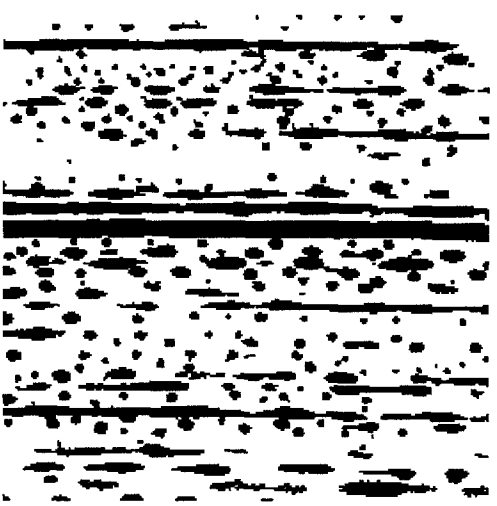

Figure 3: *Binary* image corresponding to figure 1

Characterization of the image in figure 3 consisted of two steps. We first sorted all particles that originated from the same fiber's segmentation into families and measured the distances between the centers of the particles belonging to the same family. We then estimated the initial radius of the fibers that produced the previous families of particles.

3.1.1. b) Transformations of the *binary image*

For sorting particles according to their origin, one had to remember that:

- Alignments were parallel to each other. The direction of alignment was taken as the horizontal of image (see figure 3);
- The spacing between particles born from the same fiber were perceptibly equal;
- The sizes of particles born from the same fiber were about equal.

For *labelling* the *cells* of *binary* image, three criteria were applied:

- The first consisted in computing the linear *distance function of the matrix,* in the direction of alignment of the particles;
- The second consisted in estimating the *cell*'s size. This was done by taking the size of the maximum hexagon included in the *cell* as the size of the *cell* (starting from a *granulometry).*
- The third, which leds to the best result, is described below.

3.1.1. c) Algorithm for *labelling* aligned *cells*

The principle was to use the *thick skeleton* that gave a reliable indication of the location of the medial axis of particles. The basic idea for *labelling* the particles belonging to the same family was to identify as lines of alignment the horizontal lines that intersected the maximum length of *thick skeleton*. (See process chart Appendix B).

3.1.2. Estimation of the initial characteristics of fibers

After the calculation of the length λ associated with each fragmentation, we tried to estimate the initial fiber radius as a function of the characteristics of particles after breakup, and to verify the relation between λ and R_o (relation 2).

We used the following hypotheses:

- The initial fiber volume and the sum of volumes of particles that originated from the breakup of fiber were equal;
- Initial fibers were assumed to be cylindrical in shape, particles after breakup were taken as elongated ellipsoids.

This led to the following comments:

- The apparent dimensions of fragments on the analyzed image were not the real ones. The thickness of the samples for transmission electron microscopy observations was of same order of magnitude as that of the small spherical particles. One can show that, in the most unfavorable case, the probability that the apparent radius was included in the 0.75 R_o - 1.0 R_o range is 0.70 (in the case of a spherical particle);
- Although the real value of radius was not known, we calculated the apparent volume of particles assuming these particles were ellipsoid with dimension equal to the apparent one;
- The major axis of the ellipsoid was taken as equal to the horizontal *Feret diameter* of the particle, the minor axis was taken equal to the vertical *Feret diameter*. The area of the ellipsis defined by the two *Feret diameters* was generally larger than the digital area of the particle.

We were then able to calculate the apparent radius $R_{o\,app}$ of mother fibers. We have plotted, on figure 4, $R_{o\,app}$ as a function of λ.

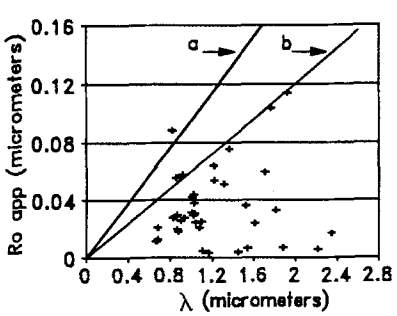

Figure 4: Plot of $R_{o\,app}$ in function of λ, (a) curve corresponding to rel. 2, (b) estimation curve (see text)

As $R_{o\,app}$ was underestimated, all experimental points (except one) lied below the line defined by equation (2), as expected. When we looked more precisely at the location of experimental points, we remarked that they were divided into two groups:

The results were commented as follow:

- A first group of points lied under, but not far from, a straight line running through the origin of axes and the slope of which was lower than the one defined by equation (2) (see figure 4).
- A second group of points fell

along the x axis. These points corresponded to fibers whose initial radii were small. The length associated with their breakup seemed to be independent of the initial fiber radius.

To explain that all experimental points of the first group lied below a line of lower slope than the line defined by equation 2 one had to take into account that:

- The underestimation of R_0 led to lower the ordinate of experimental points on figure 4. The magnitude of diminution depended on the position of the particle in the depth of the sample.
- The theory of Tomotika is applicable for Newtonian liquids (14,15). For our non-Newtonian system the A value could be different (16), although Pakulta *and al.* (17) have reported good agreement with Tomotika's theory in kinetic of breakup of different polymers blends.

A better agreement with the experimental results would be obtained by substituting line (b) with line (a) in figure 4. However the value of p associated with this line would differ for more than a factor 20 from the admitted one. That seemed improbable.

To explain the position of the second group of points we noticed that Elmendorp (14) reported that when R_0 is small, fibers could have been deformed by an elongation of the matrix. In these conditions the breakup did no longer obey the Rayleigh mechanism. The distances between the centers of the particles were greater than predicted by Rayleigh's theory.

3.2 Analysis of the mode of breakup with a *covariogram*

We also tried the method based on the *covariance* function (6,8) to check if the morphology could be explained by a Rayleigh mechanism and to calculate the associated length λ.

To demonstrate the possibilities of the *covariance* analysis we computed the *covariogram* of each of the two alignments chosen in figure 3 and reproduced in figure 5. This computation was available with a user module, which we added to *Visilog*. The *covariograms* are plotted in figure 6 as curve (b) and (c) respectively.

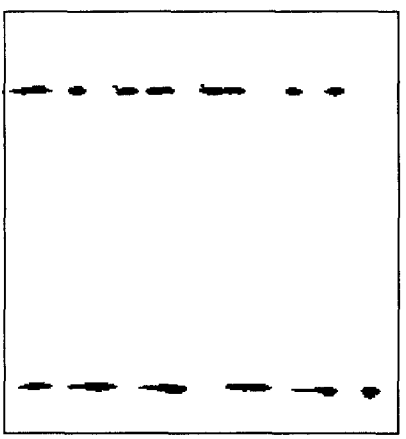

Figure 5: *Binary* image of two alignments

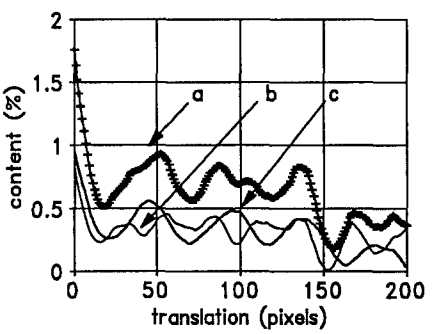

Figure 6: *Covariogram* of image represented on figure 5 (a) both alignments, (b) first alignment, (c) second alignment

If the dispersion of particles obeys the Rayleigh mechanism, four characteristics of the *covariogram* should be observed (see figure 6 - curve b and c).

- The *covariogram* computed in the direction of alignment should show periodicities, the interval between two maximas being equal to the length λ associated with the breakup (the initial value of the *covariogram* is the first maximum);
- The interval between a maximum and a minimum is then equal to the mean length of the particles ;
- The slope at origin is directly related to the number of particles per unit of length;
- The damping of the *covariogram* gives information about the regularity of the breakup.

The *covariograms* b and c satisfied these requirements. However, when several close lengths λ_n are simultaneously present in a morphology, they can counterbalance each other, so a maximum of the *covariogram* can be less pronounced: see the *covariogram* computed using the entire image of figure 5 (curve a) in figure 6. For the same reason *the covariogram* we had computed from the image of figure 3 was difficult to interpret.

4. Conclusion

We tried to apply concepts of image analysis by mathematical morphology for analyzing a specific morphology of polymer blends, namely that of particles that originated from a Rayleigh type breakup.

We used two different methods for analyzing the morphology:

- Particles *labelling*, that allowed, with hypothesis of conservation of volume between initial fibers and observed particles after breakup, to check if the characteristics of morphology were in agreement with Tomotika's theory;
- Global analysis of morphology with a *covariogram* that allowed to quantify the morphological characteristics of a breakup following a Rayleigh mechanism.

Image analysis is, for now, not commonly used for polymer blends characterization. This attempt shows that image analysis, especially by mathematical morphology, seems to be an interesting tool for a better understanding of polymer mixing.

Acknowledgements

The authors wish to thank Peugeot S.A. and Renault for their financial support.

References

1. Tanaka, Hayashi T., Nishi T. (1986) J. Appl. Phys. 59:653
2. T. Tanaka, Hayashi T., Nishi T. (1986) J. Appl. Phys. 59:3627
3. Gur Y.S., Malone M.F., Bhatia Q.S., Reynolds G., Karasz F.E., Hanson A. R., Riseman E.M. (1989) Polym. Engin. and Sc.29:1427
4. Meyer F., Gratin C. (1991) to be publ. in Proc. 8th ICS, Irvine, California
5. Wippler C., (1991) Polym. Bull. 25:357
6. Serra J. (1989) Image Analysis and mathematical morphology - volume 1 - Academic Press - ISBN 0-12-637240-3 - ISBN 0-12-637242-X
7. Serra J. (1988) Image Analysis and Mathematical Morphology - volume 2: Theoritical Advances - Academic Press - ISBN 0-12-637241-1
8. Chermant J.-L., Coster M. (1989) Précis d'analyse d'image - Editions du CNRS - ISBN 2-87682-020-X
9. Salier S. (1990) Research Report, Ecole d'Application des Hauts Polymères, Strasbourg
10. Tomotika S., (1936) Proc. Roy. Soc. (London) A153:302
11. Tomotika S., (1935) Proc. Roy. Soc. (London) A150:332

12. Rayleigh J.W.S., (1878) Math. Soc. Proc. 14:4
13. Rayleigh J.W.S., (1879) Proc. Roy. Soc. 29:71
14. Elmendorp J.J., (1986) "A Study on Polymer Blending Microrheology" PhD thesis, Techn. Hogesch., Delft
15. Elmendorp J.J., (1986) Polym. Eng. and Sc. 26:418
16 Wei-Kuo L., Kuo-Liang Y., Flummerfelt R.W. (1981) Int. J. Multiphase Flow 7:385
17. Pakulta T., Grebowicz J. and Kryszewski M. (1980) Polym. Bull. 2:799

Appendix A: definitions of various technical terms:

Gradient image: The gradient image shows the location of the areas of great contrast in a gray level image. On an image of morphology, the gradient image shows the edge of the particles in the dispersed phase.

Binarization: Initial gray level image is thresholded into two levels; one level corresponds to the dispersed phase and is set to the level 1 (represented here in black), the matrix is set to the level zero (represented here in white).

Pixel: The pixel is the elementary entity in a digital picture. Each pixel is defined by its position and its gray level. In this study, images were digitalized on images of 256*256 pixels.

Cell: Connected pixels form a cell.

Labelling: Each cell on the image is set to a different gray level. In this paper the labelling was not the standard one: all the cells (particles) which come from the same fiber breakup were set to the same gray level.

Reconstruction: Reconstruction consists in propagating markers, which are set to level M, to all cells that are connected to the markers. After reconstruction, reconstructed cells are set at level M.

Top-hat transformation: Transformation of mathematical morphology that shows clearer or darker areas of the image up. In this paper top-hat transformation was used to enhance the contrast between particles and matrix.

Distance function: Function that is defined for each pixel by setting its value equal to the shortest distance from this pixel to the boundary. The linear distance function, which we added to Visilog, computes the distance function in only one direction. (horizontal direction)

Thick skelet: The skelet is defined as the set of the centers of all maximal disks that are included in the analyzed cell. A thick skelet can be obtained with a fast algorithm that uses the distance function as input image.

Feret Diameter: The Feret diameter is the diameter of the convex hull of the studied cell. Usually, the horizontal and vertical Feret diameters are measured.

Granulometry: Granulometry corresponds, in a picturesque manner, to the sifting of the studied phase with sifters of increasing sizes. The analysis uses successive image transformations with a structuring element of increasing sizes. The structuring element is generally a hexagon, digital approximation of a disc.

Covariance function - covariogram: The basic idea for the covariance function is to compare the morphology at point h, and the morphology at point h', extremity of the segment h-h' of fixed length and orientation. When h is in the dispersed phase, one tests if the point h' falls too in the dispersed phase or not.

In a practical manner, the previous transformation, which is called erosion by a bipoint h-h', is obtained by a translatory motion of the original image by h-h' in the direction of analysis. Then a

logical "and" operation is computed between original and shifted image. The point h belongs to the original image, while h' is the corresponding point belonging to the shifted image. The remaining points after transformation are those for which h and h' fall in the dispersed phase.

The covariogram is the plot of the area of the output image for increasing sizes of the structuring element h-h'. The measured area is corrected for the change of size of the analyzed field as the size of the segment h-h' is increased.
The covariogram shows the organization of morphology. The initial value of the curve indicates the percentage of dispersed phase, the covariogram tends to the square of the initial value. Between initial and asymptotic value, the covariogram will be flat if the morphology is at random or will show oscillations if periodicities are present in the morphology.

Image analysis software: Visilog was used for this study. Visilog was created by NOESIS (NOESIS SA - Vélizy - France). For the analysis of polymer blends we programmed different additional modules in C language and linked them to the software.

Appendix B: Process chart of module designed for labelling of particles as a function of alignment

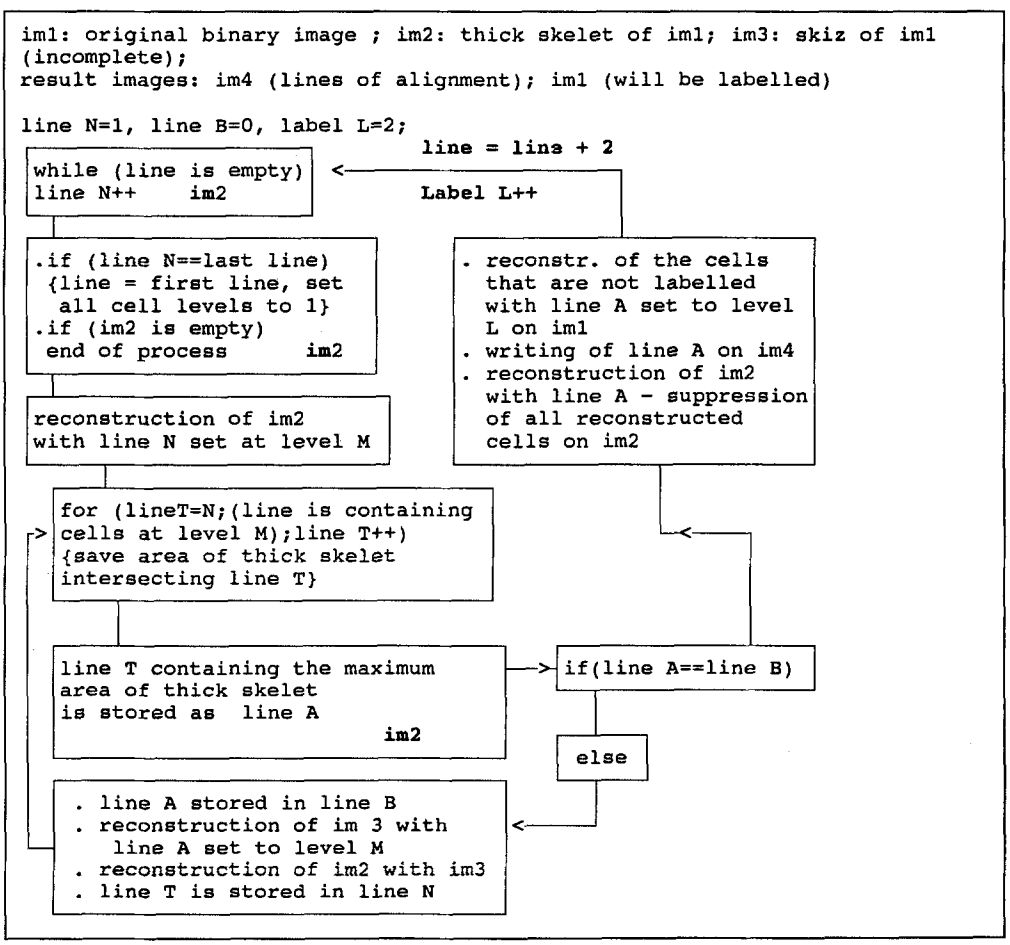

Accepted February 5, 1992 C